Journal of Ionic Liquids 3 (2023) 100053

Contents lists available at ScienceDirect

Journal of Ionic Liquids

journal homepage: www.elsevier.com/locate/jil

Kinetic analysis of an ionic liquid-based metal extraction process using a single droplet extraction column

Enas A. Othman[a,b,*], Aloijsius G.J. van der Ham[b], Henk Miedema[a], Sascha R.A. Kersten[b]

[a] Wetsus, European Centre of excellence for sustainable water technology, Oostergoweg 9, 8911 MA Leeuwarden, The Netherlands
[b] Science and Technology Department, University of Twente, Drienerlolaan 5, 7522 NB Enschede, The Netherlands

ARTICLE INFO

Keywords:
Ionic liquids
Solvent extraction
Metal extraction
Mass transfer
Reaction kinetics
Single droplet extraction column
Statistical cross-validation method

ABSTRACT

In this study a liquid-liquid extraction (LLX) process has been investigated based on experimental analysis and kinetic modelling. The purpose of this investigation is (1) to understand the mass transfer behaviour, (2) to determine the rate limiting step via evaluating different mass transfer models, and (3) to estimate the mass transfer and kinetic parameters. This has been discussed in the context of the extraction of Co by the ionic liquid (IL) $[P_{8888}][Oleate]$ as an example of LLX with chemical reaction. Mass transfer models, with and without a chemical reaction, are evaluated based on a statistical cross-validation method. The following operational parameters are included in the analysis: column lengths, droplet diameter, droplet rising velocity and continuous and dispersed phase concentrations on Co uptake. This method reveals that a single parameter representing the external mass transfer resistance can describe the forward extraction of Co (i.e., into the IL) for the whole data set sufficiently accurate (error ±30%) regardless of the studied operational conditions. Back-extraction of Co from pre-loaded IL droplets shows a different transfer mechanism. Now the mass transfer in the dispersed IL phase dominates the process which is attributed to a change of the physical properties of the pre-loaded IL.

1. Introduction

Extraction columns are widely used in chemical, hydrometallurgical, petrochemical, and pharmaceutical separation processes due to their low energy consumption, high efficiency and simplicity of operation (Huang et al., 2016; Anari et al., 2018; Rahbar et al., 2011). However, lack of knowledge regarding hydrodynamics, mass transfer, chemical kinetics and the underlying thermodynamics limits the optimization of these columns. One reason for this is that studying the extraction process on large scale is expensive and time-consuming since it requires rather large quantities of chemicals and a large number of pilot experiments. Using a single droplet extraction column is a promising method to investigate mass transfer behaviour in LLX system (Jie et al., 2005).

Metal extraction, representing a conventional industrial process, can be considered a general framework for studying mass transfer combined with reaction in columns. This type of investigations is usually performed using $ZnSO_4/D_2EHPA$/Kerosene, which is recommended by the European Federation of Chemical Engineering as a standard test system (Anari et al., 2018; Korb et al., 2018). The present study focuses on the extraction of Co due to its significant value in supporting economic growth and development next to reducing environmental impact arising from metallurgical, and mining industries (Cheng et al., 2019; Othman et al., 2019). In this study, $[P_{8888}][Oleate]$ is used which demonstrates a high and selective extraction efficiency towards Co over several consecutive batch cycles (Othman et al., 2019; Parmentier et al., 2015). The presence of bulky, long-chained tetraalkylphosphonium cations and hydrophobic oleate anions minimizes the loss of IL to the aqueous phase.

The rate of LLX with chemical reaction is a complex function of mass transfer rate and chemical reaction kinetics. Mass transfer and chemical reaction occur at or across the interface of each droplet where fluid dynamics and mass transfer are inseparably associated with interfacial properties and phenomena, such as droplet deformation, internal circulation, oscillation or Marangoni instabilities, amongst others (Wegener et al., 2014). Mass transfer can be described by the two film theory, penetration theory or surface renewal theory (Lo et al., 1983). Reactive extraction is defined by a chemical reaction which occurs either at the interface “Heterogeneous reaction” or within the bulk phase “Homogeneous reaction”. For a heterogenous system, two extreme conditions exist regarding the rate controlling mechanisms of the extraction:1) the diffusional regime where the mass transfer controls the extraction rate and 2) the chemical regime in which the kinetics of the chemical reaction is controlling. A reaction in the bulk results in a higher capacity as the extracted solute is “stored” by the chemical reaction and it can maintain the high initial flux for a longer period of time as it reduces the concentration of “free” solute.

In a single droplet extraction column, the estimation of the mass transfer coefficients depends mainly on the knowledge of mass transfer behaviour Huang et al., 2016). Even though, a large number of studies

* Corresponding author.
E-mail address: e.a.othman@utwente.nl (E.A. Othman).

https://doi.org/10.1016/j.jil.2023.100053
Received 27 August 2022; Received in revised form 24 April 2023; Accepted 8 May 2023
2772-4220/© 2023 The Authors. Published by Elsevier B.V. This is an open access article under the CC BY-NC-ND license (http://creativecommons.org/licenses/by-nc-nd/4.0/)

Nomenclature

Symbols

a:	Specific interfacial area $\left(\frac{6}{d}\right)$ [m^2/m^3]
B_n:	n^{th} coefficient in the equation of Kronig-Brink/ Gröber [-]
C:	Concentration [M]
C_{Co}:	Solute concentration free (Co) [M]
C_{CoCl_2}:	Solute concentration free ($CoCl_2$) [M]
C_{CoCl_2-IL}:	Solute concentration complexed with IL [M]
$C_{CoCl_2,Total}$:	Total Solute concentration (free and complexed with IL) [M]
C_{IL}:	IL concentration free [M]
$C_{IL,total}$:	IL concentration both free and complexed with $CoCl_2$ [M]
CC:	Cross correlation matrix [-]
CV_5:	5-fold cross validation [-]
X:	Distribution coefficient [-]
D_i:	Diffusion coefficient [m^2/sec or cm^2/sec]
D:	Droplet diameter [m]
E_a:	Activation energy [kJ/mol]
J:	Flux [mol/m^2]
K:	Overall mass transfer coefficient [m/sec]
k:	Partial mass transfer coefficient [m/sec]
K_{cc}:	Average correlation value of the cross-correlation matrix [-]
K_{eq}:	Equilibrium constant (Homogenous reaction) [-]
$k_{eq,int}$:	Equilibrium constant (Heterogenous reaction) [-]
k_r:	Reaction rate constant (Homogenous reaction) [1/M^2sec]
$k_r^{\pm}$:	Forward and backward reaction rate constant (Heterogenous reaction) [1/M^2sec]
m:	Partition coefficient [-]
MSE:	Mean square error [-]
n:	Indices [-]
N:	Number of experiments [-]
N_P:	Number of parameters [-]
P_i:	Fitted parameter of the MSE_{best} fit [-]
Pe:	Peclet number $\left(\frac{du}{D}\right)$ [-]
R:	Gas constant 8.31446 [J/mol K]
r:	Reaction rate [M/sec]
Re:	Reynolds number $\left(\frac{\rho u d}{\mu}\right)$ [-]
Sc:	Schmidt number $\left(\frac{\mu}{\rho D_i}\right)$ [-]
Sh:	Sherwood number $\left(\frac{kd}{D_i}\right)$ [-]
T:	Temperature [K]
t:	Residence time [sec]
u:	Slip velocity [m/sec]
V:	Droplet volume [m^3]
wt:	Weight fraction [%]

Greek letters

λ_n:	n^{th} Eigen values in the equation of Kronig-Brink/ Gröber [-]
ρ:	Density [kg/m^3]
σ_{Pi}:	Standard deviation of each parameter over the 5 fits [%]
$\sigma_{P,avg}$:	Average standard deviation of a model over 5 fits [%]
μ:	Viscosity [Pa.sec]
κ	Viscosity ratio $\left(\frac{\mu_d}{\mu_c}\right)$

Superscripts

c	Continuous phase
d	Dispersed phase
n	Number of anions
*	Equilibrium

Subscripts

Aq:	Aqueous
c:	Continuous phase
d:	Dispersed phase
in:	Inlet
int:	Interface
n:	Number of anions
exp:	Experimental

Abbreviations

Co	Cobalt
Exp	Experimental
IL	Ionic liquid
LLX	Liquid-liquid extraction

can be found in literature with respect to theoretical models and empirical correlations for predicting the mass transfer coefficients, the predictions show both success and failure when compared with experimental results (Huang et al., 2016; Kumar and Hartland, 1999; Chen et al., 2015). Moreover, it is usually claimed that it is difficult to assess the predictive ability of literature correlations, since the range of their applications is not always known (Kumar and Hartland, 1999). This introduces extra difficulty in selecting the right model. Kumar and Hartland have published a collection of mass transfer correlations for a rising droplet (Kumar and Hartland, 1999). Mass transfer correlations for the continuous phase are expressed in the form of $Sh_C = f(Re, Sc_c, \kappa)$ where κ is the viscosity ratio between the dispersed and continuous phase. Several mass transfer models and correlations into and out of a droplet have been frequently applied, all with their respective boundary conditions. The Newman model applies to rigid spherical droplets without internal circulation (Newman, 1931). The mass transfer intensifying effect of droplet internal circulation is taken into account by ((1) Kronig-Brink who proposed a model for laminar diffusion with internal circulation and (2) Handlos-Baron who proposed a model in which a turbulence-like disturbance is added to the internal circulation (Wegener et al., 2014; Handlos and Baron, 1957; Kronig and Brink, 1951). To overcome the limited prediction of the Newman model, Zheng et al., implemented an enhancement factor reflecting the effect of initial solute concentration, droplet rise velocity and interfacial instability (Steiner, 1986; Zheng et al., 2014). Wegener et al., improved the Handlos-Baron model by introducing a concentration dependant parameter accounting for the influence of the initial solute concentration difference between the aqueous and organic phase and to characterize the intensity of the Marangoni effect (Wegener and Paschedag, 2011). Anari et al., developed a correlation for an effective diffusion coefficient to reveal the effect of chemical reaction on mass transfer rate (Anari et al., 2018).

In this paper we investigated the mass transfer and reaction kinetic of Co extraction by $[P_{8888}]$[Oleate] to determine the rate limiting step and to evaluate whether adding a chemical reaction to the mass transfer model is necessary to describe the forward and backward extraction. Furthermore, we have also examined whether the stagnant and internal circulation models and correlations found in the literature provide a satisfactorily prediction of the experimental data. The two-film theory has been applied to predict Co uptake using (1) an internal circulation model and correlation from literature, and (2) a mass transfer model with and without chemical reaction using a statistical cross-validation (CV_5) method. Both options are evaluated. The CV_5 method is applied as described in the work of Slotboom et al., (Slotboom et al., 2020). It permits the calculation of associated mass transfer and kinetic parameters, and with that it identifies the rate limiting step(s) of the overall process. This is achieved via studying the extraction of Co into single IL droplets rising in a single droplet extraction column with consider-

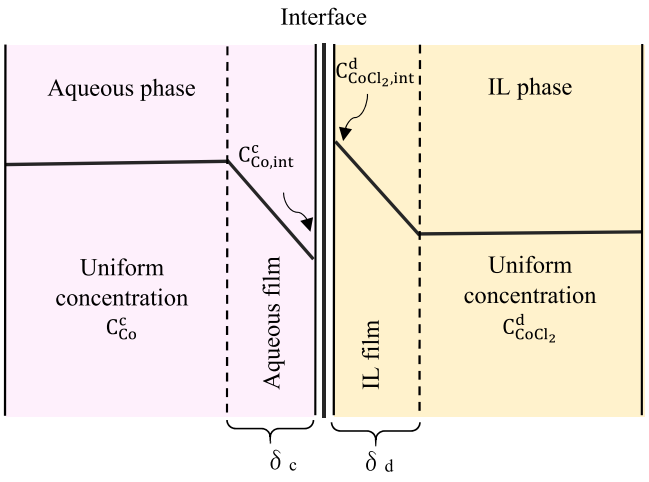

Fig. 1. Schematic representation of the two-film theory. Superscript c and d refer to the continuous and dispersed phase, respectively; the subscript int refers to the concentration at the interface.

ations for equilibria, molecular diffusion, convective mass transfer and reaction kinetics. The experimental data set consists of more than 50 experiments under different experimental conditions regarding column lengths, droplet rise velocity (both affecting the contact time), droplet diameter, and continuous and dispersed phase Co concentration. This lumped data set was then fitted by different models using the statistical cross-validation method as selection tool evaluating the predictive capability and variance of each model.

2. Theory

There are different theories concerning mass transfer between phases, such as the two-film theory, the penetration theory, and the surface renewal theory. In this study, the two-film theory was used to model the physical mass transfer of Co from the aqueous phase into the IL droplet phase. This theory was first developed in 1924 by Lewis and Whitman and it hypothesizes the existence of a distinct interface between the two phases, covered by a film with thickness (δ) on both sides of the interface Lewis and Whitman, 1924). The theory involves the following assumptions: ((1) mass transfer occurs by molecular diffusion across the films; (2) bulk concentration in both phases is homogeneous with respect to solute beyond this film; (3) mass transfer across the film occurs under steady state conditions (Morsi and Basha, 2015; Welty et al., 2009). Accordingly, for convective mass transfer, the concentration profile across the film is linear as shown in Fig. 1 (neglecting the curvature effect of the droplet since $\delta <$ d). Many transport processes involve the mass transfer of molecular species coupled to the disappearance or appearance of the particular species through a heterogeneous and/or homogeneous chemical reaction.

In this paper, three possible cases were considered regarding the transfer of Co from the continuous phase to the IL droplet. In the first case, a mass transfer model has been evaluated assuming that all the extracted $CoCl_2$ is present in the dispersed phase as free salt and that there is no reaction between the extracted salt and the IL. In the last two cases a mass transfer model has been evaluated assuming that $CoCl_2$ diffuses into the dispersed phase as a free salt and then reacts with the IL (i.e., $CoCl_2$ is present in the dispersed phase as free salt and as complex with IL). These cases are:

1. Mass transfer model using a variable distribution coefficient X (assuming no reaction between $CoCl_2$ and IL). This model has been evaluated using literature correlations for mass transfer coefficients with internal circulation.
2. Mass transfer model using m (assuming that the homogenous reaction is slow relative to the mass transfer in the time frame of the extraction). This model has been evaluated (i) using literature correlations for mass transfer coefficients with internal circulation and (ii) using the CV_5 method for estimating the mass transfer coefficients.
3. Mass transfer with homogenous reaction model using m (full model). This model has been evaluated using the CV_5 method for estimating the mass transfer and kinetic coefficients.

Using a single droplet extraction column as a prototype, the process of mass transfer has been modelled using a non-stationary mass balance with Co transferred as neutral, partially hydrated salt $CoCl_2$ into an IL droplet of specific surface area a. Here, it is assumed that $CoCl_2$ is formed instantaneously at the interface within the aqueous phase before entering the IL phase. Assuming that the single droplet is a rigid sphere, Co or actually $CoCl_2$ uptake is calculated based on the overall driving force, i.e., the difference between the equilibrium concentrations of the free $CoCl_2$ at the interface (*), defined in Eq. (3), and actual free $CoCl_2$ in the bulk IL:

$$\frac{dC^{d}_{CoCl_2}}{dt} = K\ a\left(C^{*d}_{CoCl_2} - C^{d}_{CoCl_2}\right) \tag{1}$$

Where, the overall mass transfer coefficient K is defined as the follows:

$$\frac{1}{K} = \frac{m}{k_c} + \frac{1}{k_d} \tag{2}$$

The partitioning coefficient m, which is defined as the ratio of the equilibrium concentrations of the free $CoCl_2$ at the interface. Which, at equilibrium, equals the free $CoCl_2$ salt in the dispersed phase ($C^{*d}_{CoCl_2}$), and the total Co in the continuous phase (C^{*c}_{Co})), is expressed as shown in Eq. (3). The overbars represent the organic phase.

$$m = \frac{\left[\overline{CoCl_2}\right]}{\left[Co^{2+}_{aq\ Total}\right]} = \frac{C^{*d}_{CoCl_2}}{C^{*c}_{Co}} \tag{3}$$

After the formation of $CoCl_2$, the metal salt diffuses into the bulk of the organic phase where it exhibits a homogenous interaction with the IL via replacing the hydrated water molecules of the neutral metal salt by the anion available in the organic phase (i.e., carboxyl group) to form negatively charged metal complexes that electrostatically interact with the organic cation. This hypothesis is consistent with a recent study which describes the metal extraction process as a series of elementary thermodynamic steps (Lommelen et al., 2019). The hypothesized complexation reaction between $CoCl_2$ and IL presented in Eq. (4).

$$\overline{CoCl_2} + 2\overline{[P_{8888}][Oleate]} \rightleftharpoons \overline{([P_{8888}][Oleate])_2CoCl_2} \tag{4}$$

The corresponding equilibrium constant K_{eq} for the formation of $([P_{8888}][Oleate])_2CoCl_2$ is defined by Eq. (5). The total $CoCl_2$ in the IL phase includes both the free and the part complexed with IL ($[\overline{CoCl_2}]_{Total} = [\overline{CoCl_2}] + [\overline{([P_{8888}][Oleate])_2CoCl_2}]$). Likewise, the total IL includes both the free and the part complexed with $CoCl_2$ ($[\overline{P_{8888}][Oleate]}_{Total} = [\overline{P_{8888}][Oleate]} + 2\ [\overline{([P_{8888}][Oleate])_2CoCl_2}]$).

$$K_{eq} = \frac{\left[\overline{\left([P_{8888}][Oleate]\right)_2CoCl_2}\right]}{\left[\overline{CoCl_2}\right]\left[\overline{[P_{8888}][Oleate]}\right]^2} = \frac{C^{d}_{CoCl_2-IL}}{C^{*d}_{CoCl_2}\left(C^{d}_{IL}\right)^2} \tag{5}$$

The value of the equilibrium constant K_{eq} and partitioning coefficient m are obtained by fitting the extraction isotherm obtained experimentally at room temperature to Eq. (5). The homogenous reaction of Eq. (4) occurs in parallel with the mass transfer. In this case, the reaction kinetics are coupled to the mass transfer equation to calculate the free $CoCl_2$:

$$\frac{dC^{d}_{CoCl_2}}{dt} = K\ a\left(C^{*d}_{CoCl_2} - C^{d}_{CoCl_2}\right) - r_{CoCl_2-IL} \tag{6}$$

While the formation of the $CoCl_2$-IL complex ($C^d_{CoCl_2-IL}$) is calculated as shown in Eq. (7) according to homogenous reaction expressed in Eq. (4):

$$r_{CoCl_2-IL} = \frac{dC^d_{CoCl_2-IL}}{dt} = k_r\left(C^d_{CoCl_2}\left(C^d_{IL}\right)^2 - \frac{C^d_{CoCl_2-IL}}{K_{eq}}\right) \quad (7)$$

where K_{eq} is calculated according to Eq. (5).

The consumption of IL:

$$\frac{dC^d_{IL}}{dt} = -2\, r_{CoCl_2-IL} \quad (8)$$

The total Co uptake in the dispersed phase is calculated as the following:

$$C^d_{CoCl_2-Total} = C^d_{CoCl_2} + C^d_{CoCl_2-IL} \quad (9)$$

These differential equations are solved using the following initial conditions:

For the free $CoCl_2$ in the dispersed phase:

$$C^d_{CoCl_2} = C^d_{CoCl_2}\Big|_{t=0} \quad (10)$$

For the complexed $CoCl_2$ with IL in the dispersed phase:

$$C^d_{CoCl_2-IL} = C^d_{CoCl_2-IL}\Big|_{t=0} \quad (11)$$

For the IL in the dispersed phase:

$$C^d_{IL} = C^d_{IL}\Big|_{t=0} \quad (12)$$

Where $C^d_{CoCl_2}|_{t=0}$ and $C^d_{CoCl_2-IL}|_{t=0}$ are the initial concentrations of the free and complexed $CoCl_2$ in the dispersed phase, respectively, both zero in the case of using fresh IL. When using preloaded IL, the initial free $CoCl_2$ and initial $CoCl_2$-IL complex equal their equilibrium concentrations, both defined by the equilibrium constant K_{eq}. $C^d_{IL}|_{t=0}$ is the initial concentration of free IL, which equals 1.06 M in the case of using fresh IL and $(1.06 - 2C^d_{CoCl_2-IL}|_{t=0})$ in case of using preloaded IL.

The last case considered in this study is evaluated based on the assumption that all the extracted $CoCl_2$ salt in the dispersed phase is free and that there is no reaction between the extracted salt and IL. As remarked already, the partitioning coefficient m relates the Co in the continuous phase in a constant ratio to the free $CoCl_2$ in the IL. In the absence of any complexation, this ratio does not remain constant any longer but increases over time with progressive Co uptake. For that reason, the use of the distribution coefficient (X) seems more appropriate with, X defined as the ratio of total $CoCl_2$ taken up and the total Co in the aqueous phase. Note that the (equilibrium) X values can be directly derived from the equilibrium isotherm shown in Figure A.1. Since the distribution coefficient in this LLX system is variable, reflecting that Eq. (2) is not valid. Therefore, Co uptake has been calculated using a mass transfer model that employs individual mass transfer coefficient for the continuous and the dispersed phase, with the driving force in each phase directly proportional to the difference between the bulk and interfacial concentration:

$$\frac{dC^d_{CoCl_2}}{dt} = k_c\, a\left(C^c_{Co} - C^c_{Co,int}\right) \quad (13)$$

And,

$$\frac{dC^d_{CoCl_2}}{dt} = k_d\, a\left(C^d_{CoCl_2,\,int} - C^d_{CoCl_2}\right) \quad (14)$$

The solute flux out of the continuous phase equals the flux of the solute into the dispersed phase. Combining Eqs. (13) and (14), results in:

$$k_c\, a\left(C^c_{Co} - C^c_{Co,int}\right) = k_d\, a\left(C^d_{CoCl_2,\,int} - C^d_{CoCl_2}\right) \quad (15)$$

Both Co concentrations at the interface are at equilibrium and related by the extraction isotherm (Figure A.1, Appendix A). The equilibrium correlation between $C^c_{Co,int}$ and $C^d_{CoCl_2,\,int}$ in [mol/L] is obtained by fitting the extraction isotherm of Co by a 2nd order polynomial, resulting in:

$$C^c_{Co,int} = 0.7635\left(C^d_{CoCl_2,int}\right)^2 - 0.051C^d_{CoCl_2,int} + 0.0029 \quad (16)$$

Note, at equilibrium the interface concentration is equal to the bulk concentration.

2.1. Parameter estimation

The five-fold Cross-Validation (CV_5) method was used to determine the goodness of fit statistically Slotboom et al., 2020; James et al., 2013). This method involves dividing the total dataset randomly into 5 unique folds (groups) of approximately equal size. One-fold is used for validation (test set) and the remaining four folds are used for fitting the model (training set). This procedure is repeated 5 times, where each time a different group of observations is assigned to be the validation set. The main purposes behind using this method are ((1) to determine the goodness of each model in predicting data points outside of its trained dataset and, (2) to determine the deviation of the parameters when fitted on a specific dataset.

For each training set, parameter estimation was performed using the mean square error (MSE) regression method. The MSE is the average squared difference between the estimated parameter values and the actual value (obtained experimentally) as shown in Eq. (17). Global Optimization Toolbox of MATLAB® 2017b was used to obtain the global minimum. GlobalSearch is initiated with the fmincon solver and the Sequential Quadratic Programming (SQP) algorithm.

$$MSE_k = \frac{1}{N}\sum_{i=1}^{N}\left(C_{exp,i} - C_{model,i}\right)^2 \quad (17)$$

CV_5 is calculated by averaging the five MSEs of the test sets as shown in Eq. (18):

$$CV_5 = \frac{1}{5}\sum_{k=1}^{5} MSE_k \quad (18)$$

The best model is the one which can predict experiments outside the training set good rather than fit a specific dataset perfectly. In Five-fold cross-validation, a lower CV_5 value indicates a better predictive ability of the model. The selected parameters per model are the ones with the lowest MSE for the whole dataset and the corresponding MSE is called MSE_{best}. This set of parameters is considered as the absolute best model for the total dataset.

The standard deviation of each model parameter is calculated as the standard deviation over the five fits. The average standard deviation of a model over five fits is defined as the following:

$$\sigma_{P,avg} = \frac{1}{N_P}\sum_{i=1}^{N_P}\frac{\sigma_{Pi}}{|P_i|} \quad (19)$$

Where N_P is the number of fitted parameters, σ_{Pi} is the standard deviation of each parameter over the 5 fits and P_i is the fitted parameter of the MSE_{best} fit. The value of $\sigma_{P,avg}$ represents the percentage of deviation of the obtained fitting parameters of the same model when regressed five times over essentially the same dataset. The lower the value of $\sigma_{P,avg}$ the less the parameters are changing when a completely new dataset is taken, on average.

The dependency of a fitting parameter to another can be determined by the average correlation number of the cross-correlation matrix (K_{CC}) which is calculated as follows:

$$K_{CC} = \frac{1}{N_P^2}\sum_{i=1}^{N_P}|CC_i| \quad (20)$$

The value of Kcc has been calculated by setting the diagonals to zero instead of one. This provides a value of Kcc ranging between 1 and 0 for

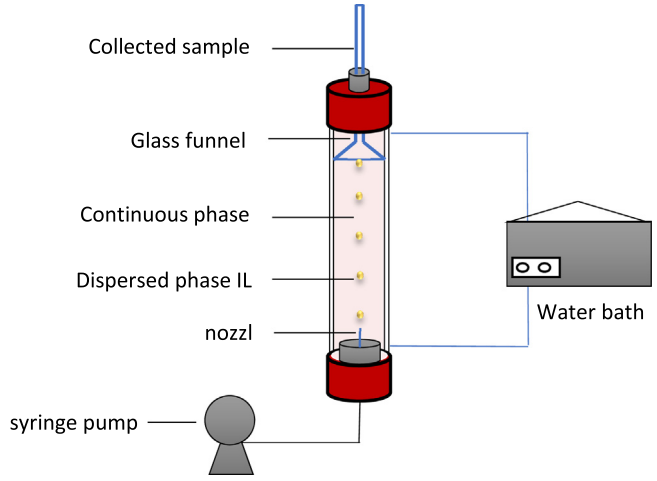

Fig. 2. Experimental setup for Co extraction measurements by single rising droplets.

any model with any number of parameters, just like the cross-correlation value itself. The closer the cross-correlation value is to 1, the higher the dependency of the fitting parameters on each other. The closer the cross-correlation value is to 0, the lower the dependency of the fitting parameters on each other.

3. Experimental

3.1. Materials and analysis

Tetraoctylphosphonium bromide (> 95%) was purchased from IoLiTec; sodium chloride, ammonium chloride, and nitric acid (69%) from VWR Chemicals; oleic acid (90%), perchloric acid (70%) and cobalt (II) chloride hexahydrate (98%) from Alfa Aesar. MilliQ water (≥18 MΩ.cm) was obtained from a Millipore Milli-Q® Biocel, which uses a Qgrade® column. All chemicals were used as received, without any further purification. Tetraoctylphosphonium oleate [P_{8888}][Oleate] was synthesized according to the procedure described by E.A Othman et al., (Othman et al., 2019).

The aqueous phases after each extraction process were analysed by a Metrohm IC Compact 761 ion chromatograph (detection range: 0.1–80 mg/L) and a Perkin Almer Optima 5300 DV inductive coupled plasma optical emission spectrometry (ICP-OES) (detection range: 0.025 - 10 mg/L). The organic phase was digested using a Milestone Ethos Easy microwave digester and analysed using the same instruments as applied for the aqueous phase. The pH and the conductivity of the aqueous and the organic phase are measured using a Mettler Toledo pH-metre with an accuracy of ±0.002.

3.2. Extraction

The mass transfer experiments were carried out in laboratory scale glass columns of different heights (50, 300, 670, 1170 and 1500 mm), as illustrated in Fig. 2. The inner diameter of the column is 18 mm which is large enough to avoid wall effects in the experiments. The column is equipped with a jacket where the temperature of the system was adjusted by an external water bath. The droplets are dosed from the bottom of the column by an Aladdin Syringe Pump, type AL1000–220. The droplets were formed at the tip of a stainless-steel nozzle with the pump running at the appropriate rate. Different nozzle sizes ranging from G8 to G23 were used to examine the effect of droplet size. G18 was selected as standard nozzle for all other experiments since it provided the smallest stable droplets at 1 ml/min. At the top of the column an inverted glass funnel was installed to collect the IL droplet in a way to minimize the interfacial area between both phases and thus reduce extra mass transfer occurring during coalescence.

In this investigation, the organic phase was chosen as the phase to be dispersed as it has a higher viscosity compared to the aqueous phase and is more expensive. The average droplet volume and diameter were determined by counting the number of droplets formed given a certain volumetric flow, while assuming all droplets to be rigid perfect spheres of constant volume. The droplet slip velocity was calculated by measuring the rising time between two defined points in the column using a stopwatch and a high-speed camera (Photron AS1, sigma 105 mm macroscopic lens). It is recommended to set the starting point at a minimum of 50 mm from the tip of the nozzle to ensure the droplet has reached a constant rise velocity (Huang et al., 2016). Each measurement was repeated at least three times. Mass transfer contact time was defined as the residence time which includes the formation time as well as the rising time.

To study the effect of Co concentration in the aqueous phase on mass transfer, fresh IL was dispersed into various column lengths containing different Co 0.02, 0.08, 0.17, 0.25, and 0.34 M (1, 5, 10, 15, 20 g/L) and equal Na concentration in g/L from their corresponding chloride salts. On the other hand, the effect of IL concentration was studied using pre-loaded IL obtained by equilibrating fresh IL with an aqueous phase containing 0.08, 0.17 and 0.25 M (5, 10 and 15 g/L) Co and equal concentration of Na in g/L from their corresponding chloride salts. Then the pre-loaded IL was injected into the 1.14 m column containing 0.08 M Co (5 g/L) and equal concentration of Na in g/L. Another set of experiments was done by pre-loading fresh IL with 0.08 M Co (5 g/L) and injecting it into columns containing 0.08, 0.17, 0.25, 0.34 and 0.42 M Co (5, 10, 15, 20 and 25 g/L) and equal concentration of Na in g/L to test the effect of pre-loading on extraction rate. ILs was preloaded via mixing the aqueous phase with equal volume of water-saturated [P_{8888}][Oleate] (around 10 wt.% water) for 10 min at 40 rpm and centrifuged (3750 rpm; 10 min, 22 °C) in an Allegra X-12R Centrifuge of Beckman Coulter.

The effect of droplet size was investigated using different nozzle sizes ranging from G8 to G23 and performed in an aqueous phase containing 0.02 M Co (1 g/L) and equal concentration of Na in g/L. All experiments were performed at room temperature unless stated otherwise. Three samples of the loaded IL were collected at the top of the column in each run, measurements and analysis was conducted as mentioned above. A specific cleaning procedure was performed following each run to avoid contamination of the system. Accordingly, all materials in contact with either the continuous or dispersed phase samples underwent multiple rounds of mechanical cleanings, subsequent rinses with acetone and deionized water, and were dried using an air blow gun.

3.3. Back extraction (regeneration)

Back extraction experiments were performed on batch scale as well as using the single droplet extraction column. In batch experiments, 5 ml preloaded [P_{8888}][Oleate] with 0.36 M Co (21 g/L) was regenerated using an equal volume of Milli-Q water. Two types of experiments were conducted. In each experiment, 5 ml Milli-Q water mixed with 5 ml preloaded IL with 0.36 M Co (21 g/L) and the total regeneration time in both experiments was 2 min. The regeneration process was performed either in one stage for the duration of 2 min (A) or in two stages of 1 min each and 30 min in between with both phases completely separated (B).

Using the single droplet extraction column, the back-extraction experiments were performed following the same procedure applied for the extraction. These experiments were conducted by first pre-loading the fresh IL with 0.34 M Co (20 g/L) and then injecting a fixed volume of this per-loaded IL into the column containing 1 M NaCl solution (25 g/L Na) to create the same environment for the transfer of Co as in the extraction experiments.

All back-extraction experiments were performed at room temperature and in duplicate. At the end of each experiment, the concentration

Table 1
Parameters employed in Eq. (21). Diffusivity of Co in the continuous phase is obtained from literature. The diffusivity of $CoCl_2$ in the dispersed phase is calculated using the Wilke Chang equation.1n as shown in (Appendix B).

Parameters	Values
Distribution coefficient (X)	2–9 (j = 0.36–1.61)
Partitioning coefficient (m)	0.9 (j = 0.16)
Diffusivity of Co in the continuous phase (D_i^c)	1.29×10^{-9} m/sec^2
Diffusivity of $CoCl_2$ in the dispersed phase (D_i^d)	4.12×10^{-11} m/sec^2

of Co in the (initially Co-free) aqueous phase was measured since the decrease of Co concentration in the IL droplet was negligible. Measurements and analysis were conducted as mentioned above.

4. Results and discussion

4.1. Modelling mass transfer in LLX

4.1.1. Conventional correlations for mass transfer coefficient with internal circulation

In this study a single droplet extraction column, where a single droplet is moving in a stationary ambient phase, was used to avoid the complexity involved in the design of multiphase dispersed systems (Wegener et al., 2014). This provides a method to investigate the extraction mechanism, to measure the mass transfer coefficient and to determine the rate limiting step. Mass transfer of a soluble component into or out of a droplet is classified based on the value of j as either dominated by an external resistance ($j >> 1$), by an internal resistance ($j << 1$) or a combination of both (conjugated resistance) ($j \approx 1$) (Huang et al., 2016; Wegener et al., 2014; Brauer, 1978). j is defined in Eq. (21):

$$j = X\sqrt{\frac{D_i^d}{D_i^c}} \text{ or } m\sqrt{\frac{D_i^d}{D_i^c}} \tag{21}$$

Where X, m, D_i are the distribution, partition and diffusion coefficients respectively. The values of X are obtained directly from the extraction isotherm while m is obtained by fitting the extraction isotherm obtained experimentally at room temperature (Figure A.1, Appendix A) according to Eq. (5). j is evaluated using (1) variable X assuming that all $CoCl_2$ in the dispersed phase is free, and (2) constant m assuming that the total $CoCl_2$ in the IL phase includes both the free and the part complexed with IL (Table 1). For the range of the studied Co concentrations, the value of j is close to 1 in the case of using distribution coefficient X, which indicates that the mass transfer resistance resides in both the continuous and dispersed phase. On the other hand, the value of j is less than 1 in the case of using partition coefficient m, which indicates that the studied system encounters an internal problem where the resistance against mass transfer resides in the dispersed phase. The value of the partitioning coefficient m = 0.9. It is worth noting that during the extraction of Co, the IL droplet exhibits internal circulation behaviour while rising in the single droplet extraction column as has been visually observed (Fig. 3). However, this effect is not taken into account in Eq. (21) which limits its applicability for a system that exhibits internal circulation behaviour.

The mass transfer coefficient in both the continuous (k_c) and dispersed phase (k_d) were calculated using the following two expressions (Kumar and Hartland, 1999):

1) Continuous phase (internal circulation droplet), the following Sherwood relation was used:

$$Sh_c = 0.6Pe_c^{0.5} \tag{22}$$

2) Dispersed phase (Kronig-Brink), the following expression for the mass transfer coefficient in the dispersed phase was used where the used Eigen-values and the values of the coefficient are listed in Table 2:

Table 2
Eigen-values λ_n and the values of the coefficient B_n used in the model of Kronig-Brink Eq. (23) (Heertjes et al., 1954; Rh and Green, 1997).

n	1	2	3	4	5	6	7
B_n	1.31	0.583	0.391	0.35	0.28	0.22	0.16
λ_n	1.60	8.62	21.3	38.5	63.0	89.8	123.8

$$k_d = -\frac{d}{6t}\ln\left[\frac{3}{8}\sum_{n=1}^{\infty} B_n^2 \exp\left\{-\frac{64\lambda_n D_i^d\, t}{d^2}\right\}\right] \tag{23}$$

The continuous and dispersed phase mass transfer coefficients are found to be $k_c = 8.6 \times 10^{-5}$–1.0×10^{-4} m/sec and $k_d = 1.8 \times 10^{-5}$ - 1.2×10^{-4} m/sec depending on both droplet diameter and contact time as listed in Table C.1 (Appendix C). Fig. 4 compares experimental Co uptake using $[P_{8888}][Oleate]$ as function of contact time and droplet diameter for different Co concentrations in the continuous phase with those predicted by the two-film theory where k_c and k_d are calculated according to Eqs. (22) and (23) respectively. The measured Co uptake (Fig. 4.A) was always lower than those predicted by the mass transfer model in the case of implementing a distribution coefficient (X) as shown in Eqs. (13–16), while assuming that all Co that is taken up remains in its free form ($CoCl_2$). The MSE for this case is 1.9×10^{-3}.

Using the partitioning coefficient m instead in Eqs. (2) and (6), assuming that there is a reaction but it is slow relative to the mass transfer in the time frame of the extraction, improves the prediction of Co uptake and reduces the MSE from 1.9×10^{-3} to 7.8×10^{-5} (Fig. 4B). This emphasizes, at least for the system studied here, the importance of using m in the two-film theory which is valid in case of having a chemical reaction, implying that the extracted metal can be present in more than one form in the extractant. Note in Fig. 4B that the model prediction starts to deviate from the experimental data at longer contact time and higher Co concentrations. More specifically the model over-predicts at short contact time and higher Co concentrations, whereas it under-predicts at longer contact time. In the literature, the deviation of the mass transfer coefficient from the value predicted by internal circulation models and correlations is attributed to surface instability (Marangoni effect) (Wegener and Paschedag, 2011; Sawistowski and Goltz, 1963). Wang et al., showed that the measured extraction fraction for the solute transferred from a hanging droplet (1-hexanol) to the aqueous phase agreed quite well with those predicted by the Kronig-Brink model at low solute concentration (Wang et al., 2011). At high solute concentration and longer contact time, the Kronig-Brink model predicts the extraction fraction fairly well only if a Marangoni-related parameter is incorporated (i.e., enhancement factor which is defined as the ratio of the experimentally obtained overall mass transfer coefficient for an ordinary drop to that for a rigid drop (see Appendix D). The incorporated enhancement factor varies based on initial solute concentration and contact time (Chen et al., 2015; Wang et al., 2011). However, this introduces an extra difficulty in developing a general model that can describe the effect of various operational conditions and hinders the understanding of the extraction mechanism of a LLX system. Fig. 4 (panel C) shows that the experimental data obtained in feed solutions containing 0.02 and 0.08 M $CoCl_2$ are relatively insensitive to the droplet diameter ranging between 2.98 and 5.28 mm. Also, in this case the model description based on the partitioning coefficient m is much better than that based on the distribution coefficient X.

4.1.2. Parameter estimation

So far, Co uptake by the IL has been modelled by employing Eq. (1), in the absence of chemical reaction. In both cases, k_c and k_d values were calculated by expressions Eq. (22) and Eq. (23), respectively. Here we

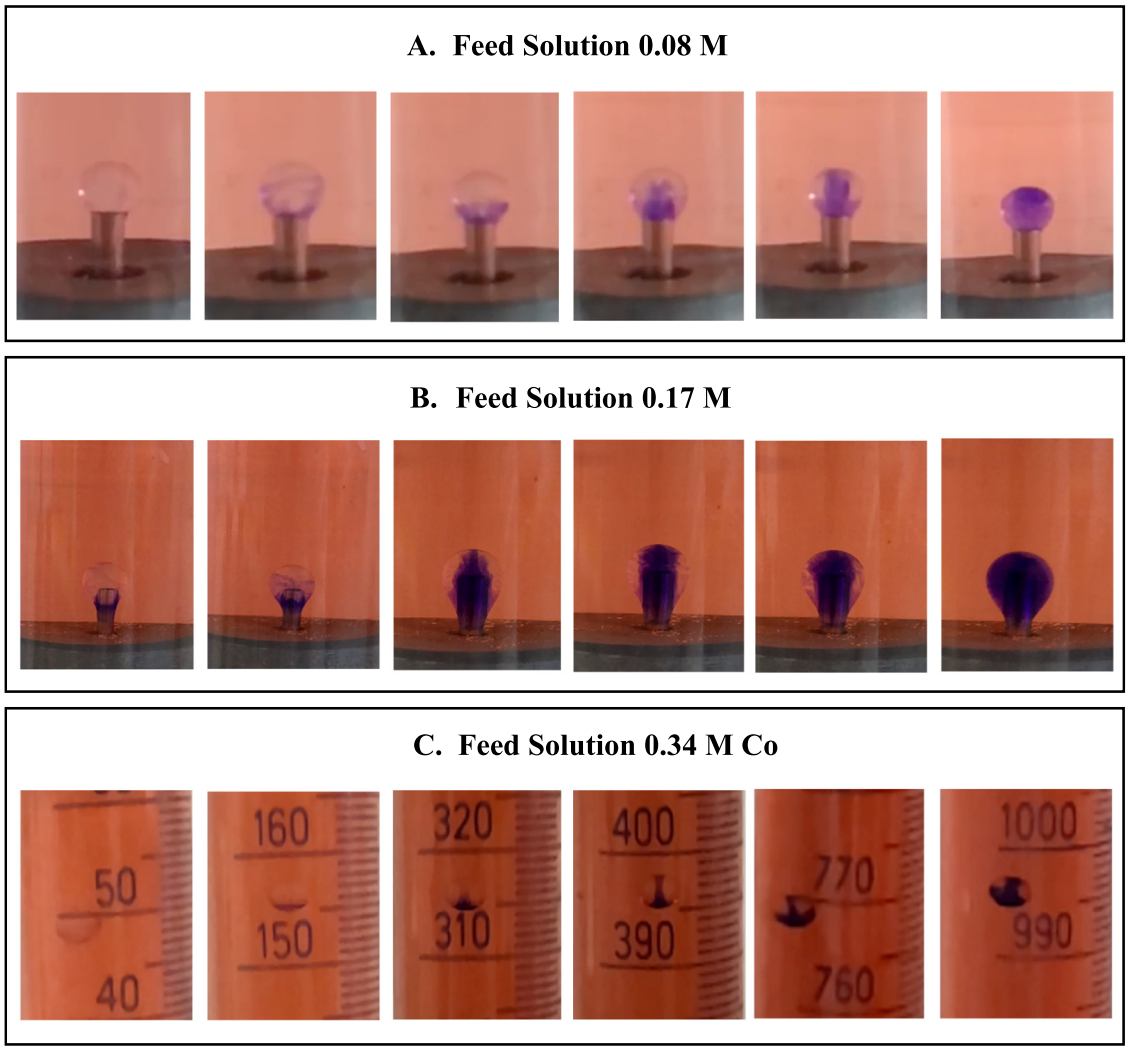

Fig. 3. Observed internal circulation within a single IL droplet hanging at the tip of the needle (panel A and B) or rising (panel C) in a single droplet extraction column at different contact times and Co concentrations in the aqueous phase (0.08, 0.17 or 0.34 M Co). Note: the higher the Co concentration in the feed or in the IL, the darker purple the droplet.

proceed with a slightly different approach, essentially based on data fitting, with the prime aim to identify the rate-limiting step. To further understand the mass transfer behaviour of Co in a LLX system and to improve the prediction of Co uptake from literature correlations, various rate models based on the two film theory with and without a kinetic reaction were evaluated. In this study, the CV_5 method is applied to (1) discriminate between different rate models, (2) determine the rate-limiting step, and (3) estimate the mass transfer and kinetic parameters. The developed models include mass transfer to and within the IL droplets as well as the homogenous chemical reaction kinetics and equilibria. These models with and without the homogenous chemical reaction are evaluated using m, since mass transfer models using literature correlations show a better prediction of Co uptake using m as discussed earlier. Regression and statistical analysis were performed employing cross validation of the different rate models and including all 52 experiments shown in Table C.1 (Appendix C). These experiments involved the effect of contact time, droplet diameter and the concentration of Co in the continuous and dispersed phase (fresh and pre-loaded IL) on the Co outlet concentration in the IL.

In total, four different extraction models (A-D) were evaluated, accounting for mass transfer with and without homogeneous chemical reaction. The first three models (A-C) without homogeneous chemical reaction are by definition mass transfer-limited. The four subcases distinguished in model A are a contribution of both an external and internal mass transfer resistance (A.1-A.4 in Table 3), in model (B) only an external mass transfer resistance and in model (C) only an internal mass transfer resistance was evaluated. The last model investigated includes homogeneous chemical reaction (D), in this particular case between the $CoCl_2$ salt and the IL. The total resistance is now a combination of a mass transfer component and a reaction kinetics component. Ignoring mass transfer resistance altogether is not discussed in this study because the total Co uptake in all experiments is much lower than the equilibrium concentration ($C^{*d}_{CoCl_2}$).

Table 3 shows the fitted parameters, regression values and statistical analysis for each of the four models. For the first three models, A, B and C, i.e., describing extraction in the absence of a chemical reaction, Fig. 5 compares the experimental and predicted Co uptake. These parity plots show that the results of the models are in good agreement with the experimental data obtained under different operating conditions, over the entire external Co concentration range and using either fresh (blue) or pre-loaded IL (red). Employing k_c and k_d in model A, shows the equal contribution of both an external and internal mass transfer resistance. Statistical analysis presented in Table 3 shows that k_c and k_d are cross correlated where K_{cc}=0.5. To reduce the cross-correlation value, model A has been re-evaluated using Sh_c and k_d as fitting parameters (A.2) or k_c and Sh_d as fitting parameters (A.3), to account for the effect of

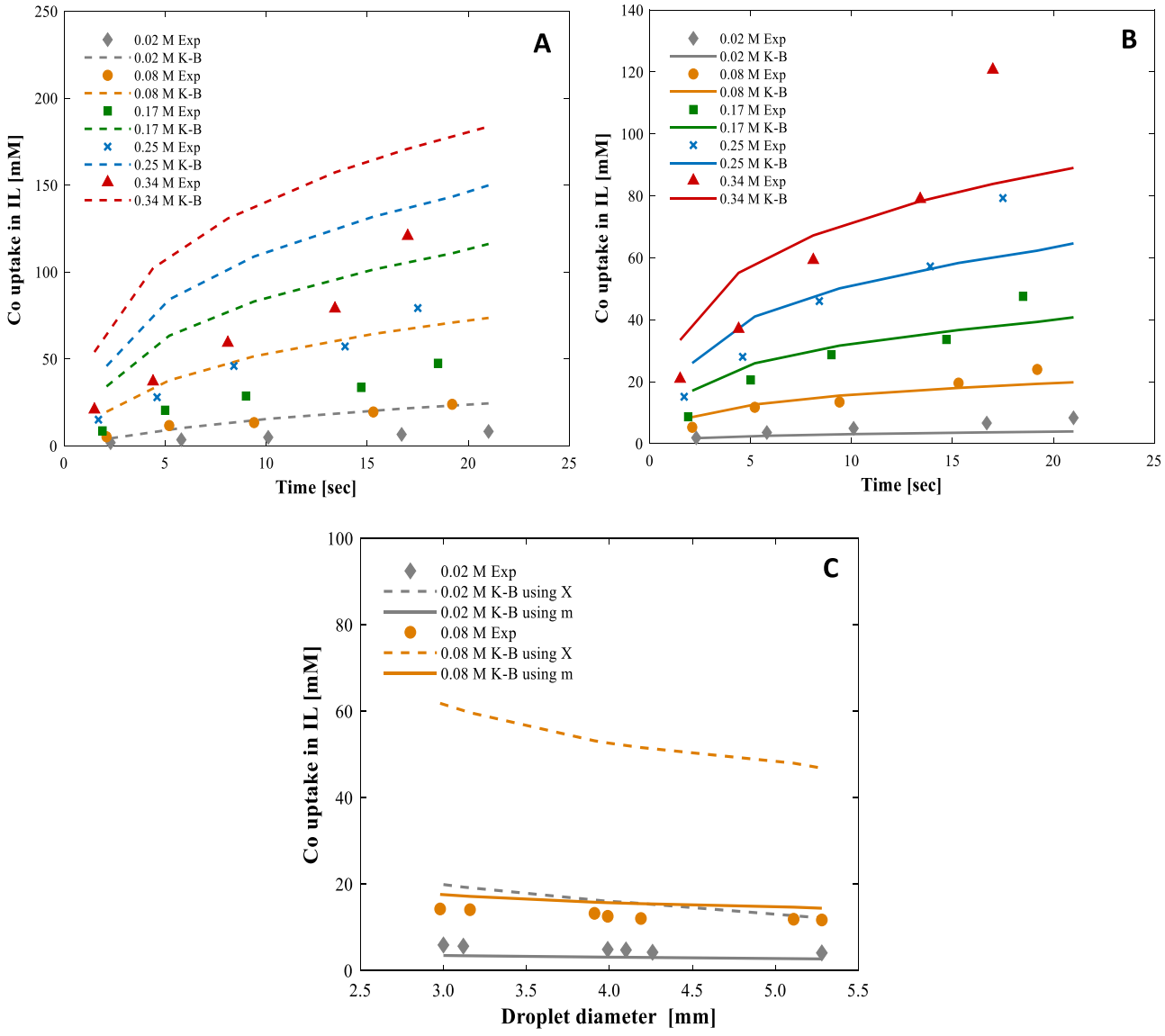

Fig. 4. Effect of contact time on Co uptake for different feed concentrations (0.02–0.34 M Co) compared with the model prediction by Kronig-Brink using either the distribution coefficient X (A) or the partitioning coefficient m (B). Panel C shows the effect of droplet diameter on measured Co uptake and the comparison with the Kronig-Brink, model using either X or m.

Table 3
The best fitting parameters out of the five runs based on MSEbest obtained for the applied different models developed using CV_5 method. The last five column on the right-hand side list the regression and statistical analysis of the fitted rate models.

Model	Fitting Parameters					Statistical analysis				
	k_c [m/sec]	Sh_c	k_d [m/sec]	Sh_d	k_r [1/M^2 sec]	CV_5	MSE_{best}	$\sigma_{p,avg}$ (%)	N_p	K_{cc}
A. External & internal mass transfer										
1. Using k_c and k_d	1.6×10^{-5}	$4.8 \times 10^{+1}$*	4.5×10^{-5}	$4.1 \times 10^{+3}$*	–	6.0×10^{-5}	5.4×10^{-5}	139.5	2	0.50
2. Using Sh_c and k_d	1.1×10^{-5}*	$3.2 \times 10^{+1}$	$3.3 \times 10^{+1}$	$3.0 \times 10^{+9}$*	–	5.8×10^{-5}	5.2×10^{-5}	72.0	2	0.002
3. Using k_c and Sh_d	9.7×10^{-2}	$2.9 \times 10^{+5}$*	1.2×10^{-5}*	$1.1 \times 10^{+3}$	–	5.8×10^{-5}	5.2×10^{-5}	248.4	2	0.19
4. Using Sh_c and Sh_d	1.1×10^{-5}*	$3.2 \times 10^{+1}$	4.2×10^{-3}	$3.9 \times 10^{+5}$		5.7×10^{-5}	5.2×10^{-5}	38.3	2	0.5
B. Only external mass transfer Sh_c	1.1×10^{-5}*	$3.2 \times 10^{+1}$	–	–	–	5.7×10^{-5}	5.2×10^{-5}	3.5	1	–
C. Only internal mass transfer Sh_d	–	–	1.2×10^{-5}*	$1.1 \times 10^{+3}$	–	17.3×10^{-5}	5.2×10^{-5}	20.9	1	–
D. Mass transfer & reaction	1.0×10^{-5}*	$3.0 \times 10^{+1}$	$5.0 \times 10^{+1}$	$4.6 \times 10^{+9}$*	2.5×10^{-1}	4.8×10^{-5}	4.8×10^{-5}	481.7	3	0.36

* k_c, k_d, Sh_c and Sh_d are calculated from the corresponding fitting parameters using the average droplet diameter (i.e., d = 3.8 mm) and the diffusion coefficients given in Table 1.

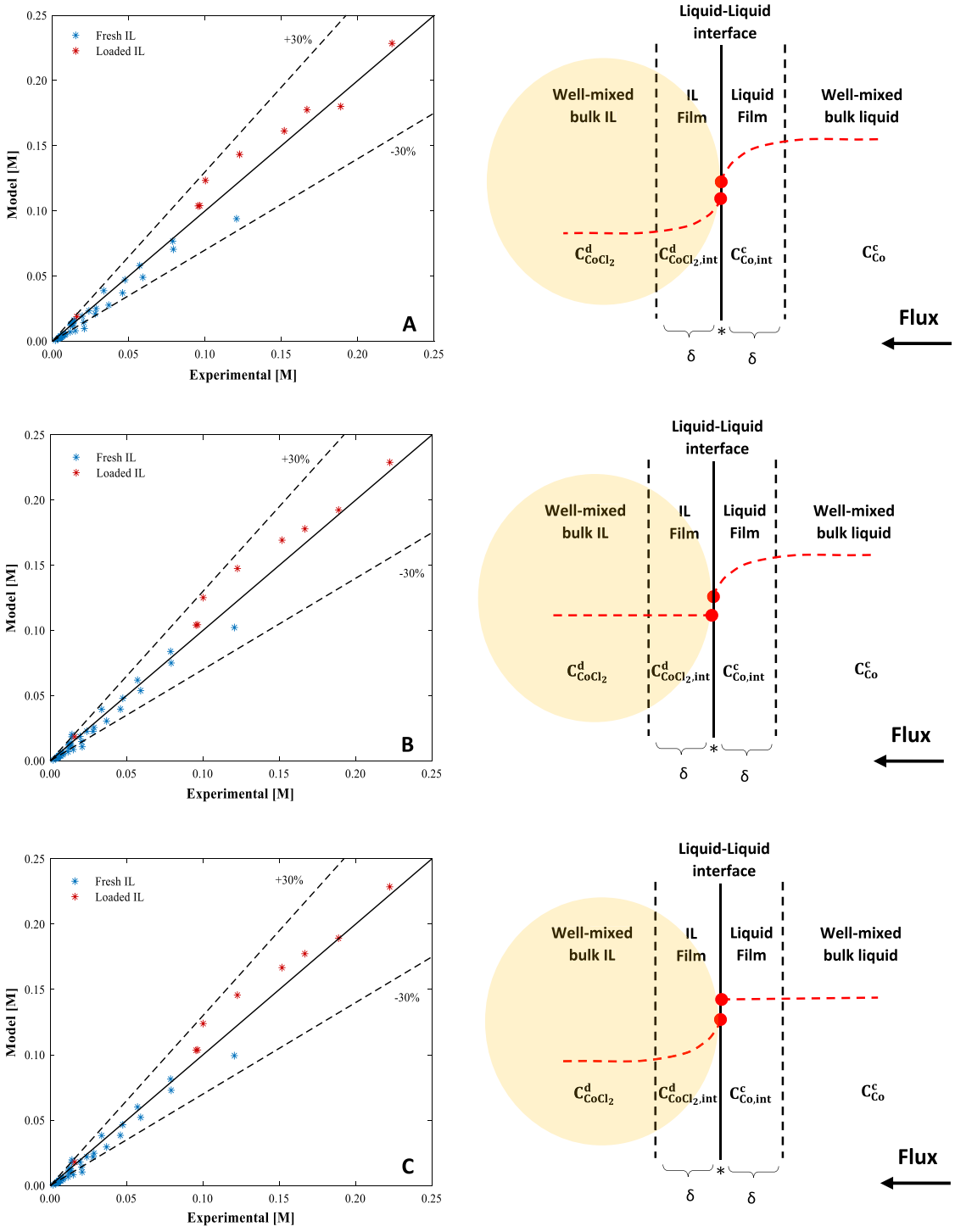

Fig. 5. Parity plots of Co uptake and concentration profile at the liquid-liquid interface where the resistance against mass transfer resides in A) both the continuous and dispersed phase B) continuous phase C) dispersed phase.

droplet diameter and the diffusion coefficient in each phase. Sh_c and Sh_d are defined according to:

$$Sh_c = \frac{k_c d}{D_i^c} \tag{24}$$

$$Sh_d = \frac{k_d d}{D_i^d} \tag{25}$$

Including Sh numbers in model A.2 and A.3 reduces the cross-correlation values from 0.5 to 0.002 and 0.19 respectively while all other statistical parameters remains unchanged as shown in Table 3. However, the system does not encounter a conjugated problem anymore and the mass transfer resistance resides in either the continuous or the dispersed phase depending on where Sh is applied. Employing Sh_c and Sh_d in model A.4, shows that the mass transfer resides in the continuous phase. However, statistical analysis shows that Sh_c and Sh_d are cross correlated like k_c and k_d used in model A.1 where K_{cc}=0.5. To clarify the effect of the mass transfer resistance in each phase, models B and C are employed where the fitting parameter is either Sh_c or Sh_d. As evident from the Sh_c value in Table 3, ignoring the internal mass

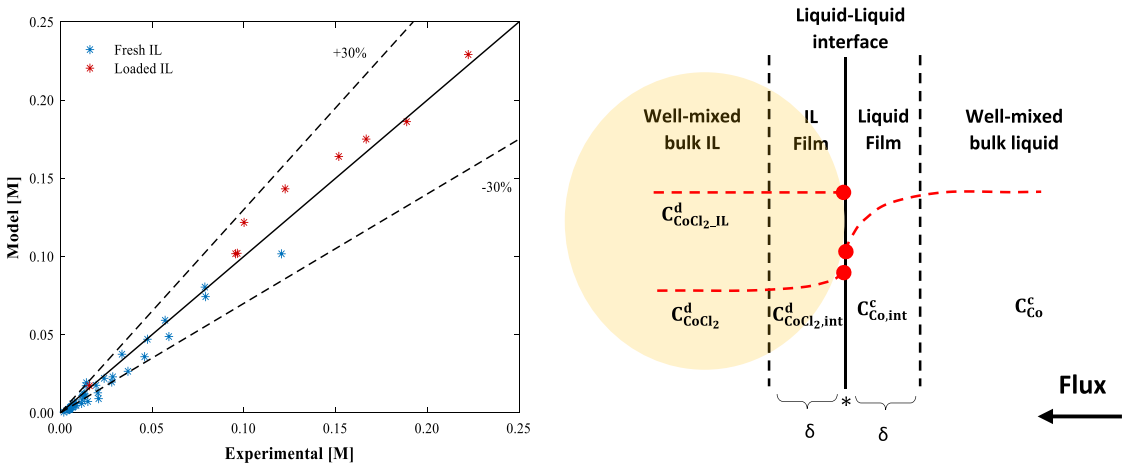

Fig. 6. Parity plots of Co uptake and concentration profile at the liquid-liquid interface for mass transfer with chemical reaction.

transfer resistance (case B) hardly affects the outcome compared to that obtained in model A.2. This conclusion is confirmed by the statistical analysis, at least regarding the values of CV_5 and MSE_{best}. On the other hand, ignoring the external mass transfer resistance (case C) reduces the predicting capability outside the training set compared to model A.3, reflecting CV_5 increases from 5.8×10^{-5} to 17.3×10^{-5}. Even though both models B and C provide a comparable fitting ability over the total dataset as evident from the MSE_{best} values in Table 3 and parity plots in Fig. 5 panel B and C, model B is preferred. Additionally, the model based on the external mass transfer resistance only (model B) provides the lowest $\sigma_{p,avg}$ which is 3.5%. This means that when a completely new dataset is considered, the fitted value of the external mass transfer resistance would have a deviation of 3.5%.

Then, the effect of adding homogenous chemical reaction to the mass transfer is examined for the extraction process as shown in Fig. 6. The values of the partitioning coefficient m and the equilibrium constants K_{eq} for the homogeneous reactions used in this model are m = 0.9 and K_{eq} = 15. These parameters are obtained from fitting the isotherm data obtained experimentally at room temperature of Figure A.1 (Appendix A) to Eq. (5). The fitting procedure minimizes the value of the mean square error (MSE) between the experimental and fitted total Co uptake. Statistical analysis listed in Table 3 reveals that the model including both mass transfer and chemical reaction has the lowest CV_5 and MSE_{best}. On the other hand, standard deviation shows a huge variation in the fitted parameters mainly k_r (3.3×10^{-4} – 8.1 ($1/M^2\,s$)).

A high $\sigma_{p,avg}$ value indicates that each of the five runs resulted in a different set of parameters, with each set of parameters still fitting with the experimental dataset. Thus, it is reasonable to conclude that models with higher $\sigma_{p,avg}$ values- although are just as good at fitting experimental data as models with lower values- don't necessarily physically reflect what is being modelled. Therefore, the lower value of $\sigma_{p,avg}$ for model B indicates that the model has a more consistent physical description (Slotboom et al., 2020). The evidence supporting this conclusion is twofold. First, considering internal mass transport only (model C) increases the CV_5 values with a factor 3. Secondly, adding reaction kinetics to the model description (model D) hardly lowers the CV_5 and MSE_{best} values compared to those models based exclusively on mass transport (models A and B). This concludes that a mass transfer model with just a single fitting parameter Sh_c (model B) can adequately describe the extraction of Co for the whole data set with most of the experimental data predicted within ±30%, regardless of the initial solute concentration in the continuous and dispersed phase, contact times or droplet diameters. The low effect of internal mass transfer resistance on Co uptake could be related to the internal circulation that is clearly visually observed during uptake in the extraction column as shown in Fig. 3.

Fig. 7 compares experimental Co uptake using $[P_{8888}][Oleate]$ as function of contact time for different Co concentrations in the continuous phase with those predicted by the two-film theory using the fitting parameter obtained in model B. The obtained fitting parameter (Sh_c) provides a better prediction of Co uptake even at long contact time and high Co concentration in the continuous phase compared to those obtained using an internal circulation model and correlations from literature as presented in Fig. 4 (panel B). The value of Sh_c obtained using model B equals 32 which is lower than the value calculated using a literature correlation (Eq. (22)) where Sh_c ranges between 251 and 307.

4.1.3. Activation energy

The determination of the activation energy is a method to distinguish between a process limited by either mass transfer or reaction kinetics. It is reported that an extraction process is diffusion-limited when the activation energy falls in the range 8–24 kJ/mol. On the other hand, the reactions contributes to the rate once it exceeds 200 kJ/mol (Scott, 2006). In order to identify the rate-limiting step during Co extraction by $[P_{8888}][Oleate]$, we applied an Arrhenius plot analysis (Cheng et al., 2019; Scott, 2016; El-Hefny, 2010). The temperature effect on the extraction rate controlled by mass transport is less pronounced than that of a process controlled by a chemical reaction (Scott, 2016). Fig. 8 shows the influence of temperature on the extraction rate of Co using $[P_{8888}][Oleate]$ in the range of 295–353 K (Appendix F). A linear correlation between $\ln dC_{CoCl_2}/dt$ and 1/T is obtained where the slope represents $-E_a/R$ according to the Arrhenius equation:

$$k_r = A\, e^{\frac{-E_a}{RT}} \tag{26}$$

The activation energy is found to be 24 kJ/mol, a value hinting in the direction of mass transfer limitation which is in line with the conclusion obtained using the model and the statistical analysis as discussed above.

4.2. Back extraction

Another important element in this study is understanding the back-extraction mechanism which is usually ignored in most studies. An earlier study by Othman et al., emphasized already the necessity of selecting the right regeneration solution and understanding its behaviour since the regeneration of the extractant and the finally obtained product are key drivers for any liquid-liquid extraction process (Othman et al., 2019). In order to investigate the back extraction, experiments were performed using $[P_{8888}][Oleate]$ preloaded with 0.34 M Co. This preloaded IL was regenerated using a 1 M NaCl solution in the 1 m single droplet column. In an extraction system completely dominated by mass transfer, extraction and back-extraction are expected to be symmetrical pro-

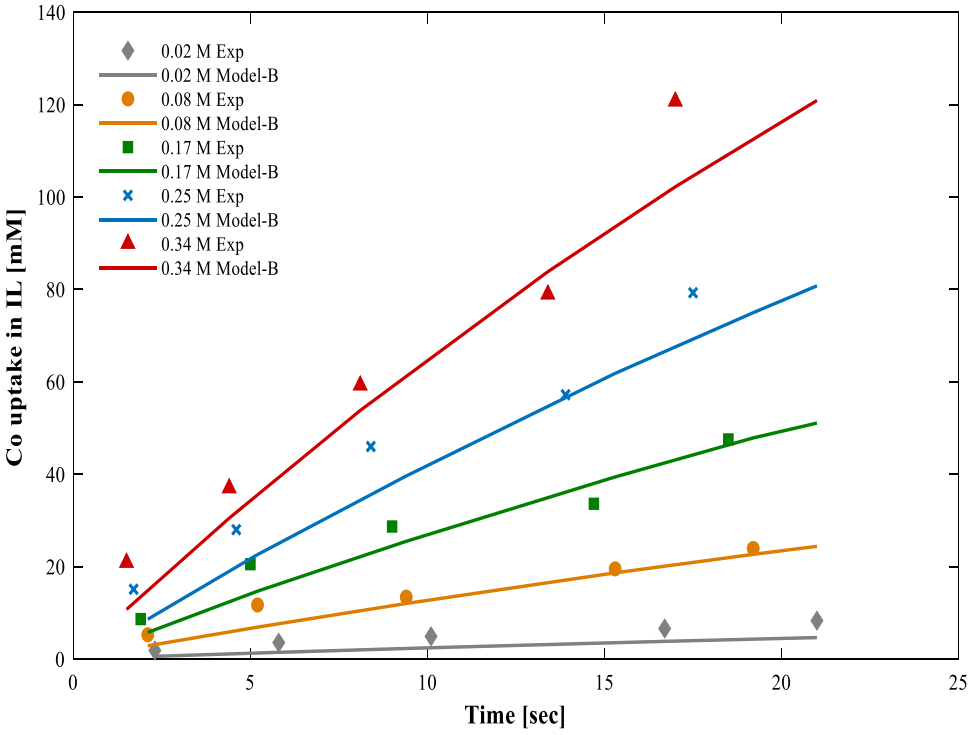

Fig. 7. Effect of contact time on Co uptake for different feed concentrations (0.02–0.34 M Co) compared with the model prediction based on external mass transfer resistance only (Model B).

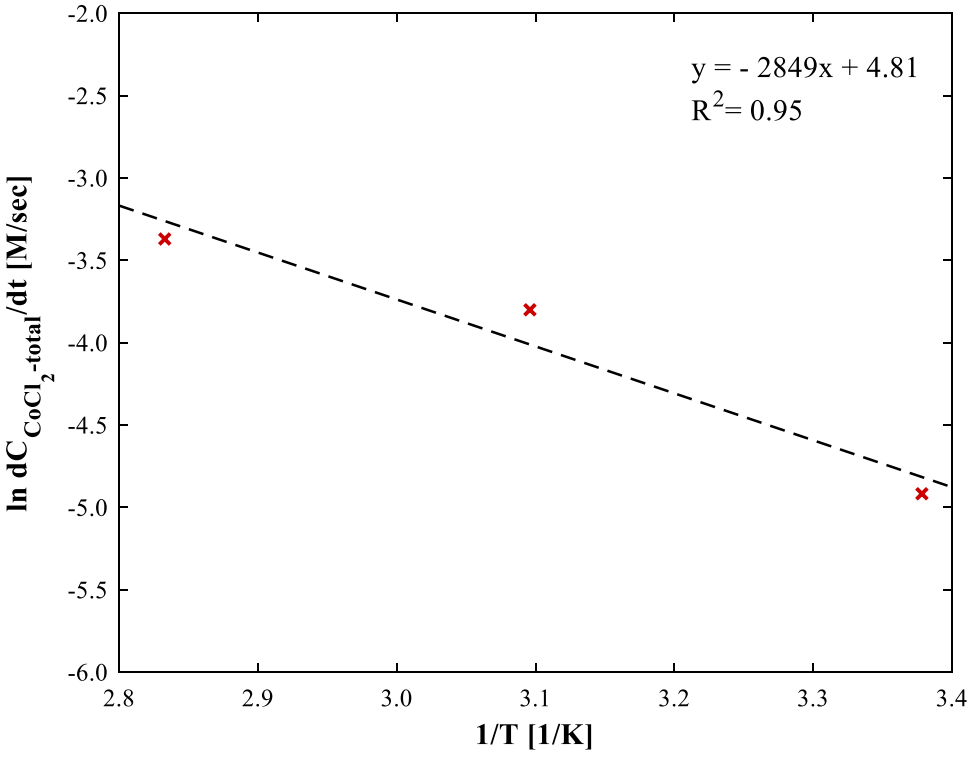

Fig. 8. An Arrhenius plot to show the effect of temperature on the extraction rate of Co using [P_{8888}][Oleate]. Co concentration in continuous phase is 0.34 M.

cesses, i.e., the calculated overall mass transfer coefficient in either direction should be the same. This hypothesis was tested by measuring the Co back extraction from IL droplets pre-loaded with Co. The measured Co in the aqueous phase was compared with the calculated concentration using the mass transfer coefficient previously derived from the extraction data. The measured concentration of Co in the aqueous phase after regeneration is found to be 0.15 mM using a 1 M NaCl solution in the column which is almost six times lower than the predicted value (i.e., 0.87 mM) assuming that back extraction is only limited by external mass transfer resistance (Table 3). This drop in the measured back-extraction rate could be related to the change of the physical properties of the IL after being complexed with the extracted Co salt. For example, the viscosity of the loaded IL shows an exponential increase as a function of the Co uptake where it increases from 0.13 Pa.*sec* in fresh IL to 0.14, 0.23 and 0.34 Pa.*sec* in IL loaded with 0.02, 0.17 and 0.27 M $CoCl_2$ respectively. This increment in viscosity of the loaded IL reduces

Table 4
Comparing the measured Co concentration in the continuous phase after back extraction with the predicted values obtained using mass transfer coefficient derived from the extraction data and mass transfer correlations for stagnant droplet.

Modelling Co concentration in continuous (water) phase	Pre-loaded Co in IL [M]	Exp. regenerated Co [mM]	Model regenerated Co [mM]
Parameter estimation from extraction	0.34	0.15	0.87
Stagnant droplet correlations			0.15

Table 5
Effect of time delay on the concentration the Co in the aqueous phase after regeneration.

Exp	Number of stages	Stage duration [min]	Time delay [min]	Aqueous phase Co [mM]
Exp_A	1	2	–	40
Exp_B	2	1	30	46

the diffusivity of Co within the IL and hinders the internal circulation observed during extraction experiments. It should be noted that for the back-extraction experiments performed in the 1.14 m column the Co uptake increased to 0.08 M at most. In the literature, it is reported that, in general, the uptake during forward extraction is higher than the release during backward extraction (Wegener et al., 2009). This is due to two reasons; first, Marangoni effects are stronger during droplet formation for the mass transfer directed into the droplet phase (forward extraction) (Wegener et al., 2009). Secondly, coalescence is more inhibited during forward extraction (Wegener et al., 2009). This latter effect can be explained by the reduced film drainage between droplet and dispersed phase at the nozzle tip due to Marangoni convection (Wegener et al., 2009).

To estimate this effect, correlations applicable to rigid, stagnant spheres, not showing any internal circulation are applied to calculate the external and internal mass transfer coefficients using the adjusted diffusivity coefficient based on the viscosity of the loaded IL which is 1.3×10^{-11} m/sec^2 as calculated based on the data shown in Appendix B. The mass transfer correlations are defined as the following:

For the continuous phase (stagnant droplets):

$$Sh_c = 2 + 0.66 Re^{0.5} Sc_c^{0.3} \tag{27}$$

For the disperse phase (Newman):

$$k_d = -\frac{d}{6t} \ln\left[\frac{6}{\pi^2}\sum_{n=1}^{\infty}\frac{1}{n^2}\exp\left\{-\frac{4n^2\pi^2 D_i^d t}{d^2}\right\}\right] \tag{28}$$

The rate model, using Eqs. (27) and (28) for k_c and k_d respectively valid for a stagnant droplet, provides a better prediction for the Co concentration in the aqueous phase after back-extraction as shown in Table 4 (i.e., 0.15 mM compared to the experimental concentration of 0.15 mM). It is worth noting that during back extraction the internal mass transfer resistance becomes dominant where $k_d = 2.8 \times 10^{-6}$ m/*sec* and $k_c = 3.6 \times 10^{-5}$ m/*sec* (Sh_c=101).

Back extraction experiments were also performed on batch scale, to verify whether the effect of a possible decomplexation reaction becomes more apparent at longer time scales. These experiments were performed using preloaded [P_{8888}][Oleate] with 0.36 M Co. The preloaded IL was regenerated using an equal volume of Milli-Q water (in the absence of NaCl to avoid any extra effect). The total regeneration time in both experiments was 2 min where the regeneration process was performed A) in one stage for the duration of 2 min, and B) in two stages each of 1 min allowing 30 min in between. This time delay is introduced to give extra time for decomplexation and formation of free Co that can be transferred from the organic to the aqueous phase during the second stage. If the back extraction would be continuously dominated by the external mass transfer, a time delay should have no influence on the amount of regenerated Co. As shown in Table 5, the introduction of a 30 min time delay resulted in 13% extra Co transfer from IL to the aqueous phase. Given an estimated experimental error of ± 0.4 mM, the effect seems significant. On the other hand, the 13% increase remains a rather marginal effect and does not justify the conclusion that the decomplexation reaction is the rate-limiting step during back extraction.

5. Conclusions

The present study focusses on the extraction of Co from an aqueous solution using single IL [P_{8888}][Oleate] droplets. The analysis investigates the mass transfer in the forward and back extraction with and without a chemical reaction and determines the rate limiting step. The results reveal that a mass transfer model with just a single fitting parameter, the Sherwood number of the continuous (aquatic) phase Sh_c, adequately describes the forward extraction of Co for the whole data set, with most of the data predicted within ±30%, regardless of the initial solute concentration in the continuous and dispersed phase, contact times or droplet diameters. The reason that the dominant mass transfer resistance during extraction resides in the continuous phase is most likely due to rather significant internal circulation inside the IL droplets, as observed experimentally. Adding a chemical reaction to the model does not improve the predictions. This is in line with the measured low activation energy of the extraction rate (E_a is 24 kJ/mol), indicating that Co uptake is indeed mass-transfer limited.

As concluded from Co regeneration from pre-loaded IL droplets, during back-extraction mass transport in the dispersed (IL) phase dominates. This may be due to a change of the physical properties (notably the increased viscosity) of the pre-loaded IL. Using correlations applicable to rigid, stagnant droplets and using a Co diffusion coefficient based on measured viscosity values, resulted in external and internal mass transfer coefficients that predicted quite well the amount of regenerated Co in the aqueous phase.

Declaration of Competing Interest

The authors declare that they have no known competing financial interests or personal relationships that could have appeared to influence the work reported in this paper.

Data availability

Data will be made available on request.

Acknowledgement

This work was performed in the cooperation framework of Wetsus, European Centre of Excellence for Sustainable Water Technology (www.wetsus.nl). Wetsus is co-funded by the Dutch Ministry of Economic Affairs and Ministry of Infrastructure and Environment, the European Union Regional Development Fund, the Province of Fryslân, and the Northern Netherlands Provinces. The authors like to thank the participants of the research theme Desalination for the fruitful discussions and their financial support.

Supplementary materials

Supplementary material associated with this article can be found, in the online version, at doi:10.1016/j.jil.2023.100053.

References

Anari, Z., Katoozi, E., Sengupta, A., 2018. Establishing correlation between effective diffusivity coefficient and the mass transfer for Zn2+ column extraction by D2EHPA: an experimental and theoretical investigation. J. Environ. Chem. Engin. 6, 6322–6327.

Brauer, H., 1978. Unsteady state mass transfer through the interface of spherical particles—II: discussion of results obtained by theoretical methods. Int. J. Heat. Mass. Transf 21, 455–465.

Chen, J., Yang, C., Mao, Z.-.S., 2015. The interphase mass transfer in liquid–liquid systems with Marangoni effect. Europ. Phys. J. Special Topics 224, 389–399.

Cheng, J., Lu, T., Wu, X., Zhang, H., Zhang, C., Peng, C.-.A., Huang, S., 2019. Extraction of cobalt (ii) by methyltrioctylammonium chloride in nickel (ii)-containing chloride solution from spent lithium ion batteries. RSC. Adv 9, 22729–22739.

El-Hefny, N., 2010. Kinetics and mechanism of extraction of Cu (II) by CYANEX 302 from nitrate medium and oxidative stripping of Cu (I) using Lewis cell technique. Chem. Engin. Process. 49, 84–90.

Handlos, A., Baron, T., 1957. Mass and heat transfer from drops in liquid-liquid extraction. AIChE. J. 3, 127–136.

Heertjes, P., Holve, W., Talsma, H., 1954. Mass transfer between isobutanol and water in a spray-column. Chem. Eng. Sci 3, 122–142.

Huang, Z., Ye, C., Li, L., Zhang, X., Qiu, T., 2016. Measurement and correlation of the mass transfer coefficient for a liquid-liquid system with high density difference. Brazil. J. Chem. Engin 33, 897–906.

James, G., Witten, D., Hastie, T., Tibshirani, R., 2013. An Introduction to Statistical Learning. Springer.

Jie, Y., Weiyang, F., Li, H.Z., 2005. Effect of packing on drop swarms extraction of high viscosity solvents. Hydrometallurgy 78, 30–40.

Korb, C., Keller, A., Bart, H.-.J., 2018. Reactive zinc extraction with D2EHPA in a Kühni miniplant column. Chem. Eng. Technol 41, 2212–2222.

Kronig, R., Brink, J., 1951. On the theory of extraction from falling droplets. Appl. Scient. Res. 2, 142–154.

Kumar, A., Hartland, S., 1999. Correlations for prediction of mass transfer coefficients in single drop systems and liquid–liquid extraction columns. Chem. Engin. Res. Des 77, 372–384.

Lewis, W., Whitman, W., 1924. Principles of gas absorption. Indus. Engin. Chem. 16, 1215–1220.

Lo, T.C., Baird, M.H., Hanson, C., 1983. Handbook of Solvent Extraction. Wiley, New York.

Lommelen, R., Vander Hoogerstraete, T., Onghena, B., Billard, I., Binnemans, K., 2019. Model for metal extraction from chloride media with basic extractants: a coordination chemistry approach. Inorg. Chem 58, 12289–12301.

Morsi, B.I., Basha, O.M., 2015. Mass Transfer in Multiphase systems, Mass transfer-Advancement in Process Modelling. InTech, pp. 189–217.

Newman, A.B., 1931. The drying of porous solids: diffusion and surface emission equations. AIChE. Trans 27, 203–220.

Othman, E.A., Ham, A.G.J.v.d., Miedema, H., Kersten, S.R.A., 2019. Ionic liquid-based process development for cobalt recovery from aqueous streams. J. Chem. Engin. Process Technol. 10.

Parmentier, D., Vander Hoogerstraete, T., Metz, S.J., Binnemans, K., Kroon, M.C., 2015. Selective Extraction of Metals from Chloride Solutions with the Tetraoctylphosphonium Oleate Ionic Liquid. Ind. Eng. Chem. Res 54, 5149–5158.

Rahbar, A., Azizi, Z., Bahmanyar, H., Moosavian, M.A., 2011. Prediction of enhancement factor for mass transfer coefficient in regular packed liquid–liquid extraction columns. Can. J. Chem. Eng 89, 508–519.

Rh, P., Green, D., 1997. Perry's Chemical engineers' Handbook. McGraw-Hill.

Sawistowski, H., Goltz, G., 1963. The effect of interface phenomena on mass-transfer rates in liquid-liquid extraction. Trans. Inst. Chem. Eng 41, 174–181.

Scott, F.H., 2006. Elements of Chemical Reaction Engineering. Prentice Hall Profesional.

Scott, H.F., 2016. Elements of Chemical Reaction Engineering. Prentice Hall.

Slotboom, Y., Bos, M., Pieper, J., Vrieswijk, V., Likozar, B., Kersten, S., Brilman, D., 2020. Critical assessment of steady-state kinetic models for the synthesis of methanol over an industrial Cu/ZnO/Al2O3 catalyst. Chem. Engin. J 389, 124181.

Steiner, L., 1986. Mass-transfer rates from single drops and drop swarms. Chem. Eng. Sci 41, 1979–1986.

Wang, Z., Lu, P., Zhang, G., Yong, Y., Yang, C., Mao, Z.-.S., 2011. Experimental investigation of Marangoni effect in 1-hexanol/water system. Chem. Eng. Sci 66, 2883–2887.

Wegener, M., Paschedag, A., 2011. Mass transfer enhancement at deformable droplets due to Marangoni convection. Int. J. Multiphase Flow 37, 76–83.

Wegener, M., Paschedag, A., Kraume, M., 2009. Mass transfer enhancement through Marangoni instabilities during single drop formation. Int. J. Heat. Mass. Transf 52, 2673–2677.

Wegener, M., Paul, N., Kraume, M., 2014. Fluid dynamics and mass transfer at single droplets in liquid/liquid systems. Int. J. Heat. Mass. Transf 71, 475–495.

Welty, J.R., Wicks, C.E., Rorrer, G., Wilson, R.E., 2009. Fundamentals of momentum, heat, and Mass Transfer. John Wiley & Sons.

Zheng, H., Ren, W., Chen, K., Gu, Y., Bai, Z., Zhao, S., 2014. Influence of Marangoni convection on mass transfer in the n-propyl acetate/acetic acid/water system. Chem. Eng. Sci 111, 278–285.